Journal of Molecular Graphics and Modelling 27 (2008) 147–160

Contents lists available at ScienceDirect

Journal of Molecular Graphics and Modelling

journal homepage: www.elsevier.com/locate/JMGM

A combination of 3D-QSAR, docking, local-binding energy (LBE) and GRID study of the species differences in the carcinogenicity of benzene derivatives chemicals

Filip Fratev *, Emilio Benfenati

Istituto di Ricerche Farmacologiche "Mario Negri", Via Eritrea, 62, 20157 Milano, Italy

ARTICLE INFO

Article history:
Received 29 November 2007
Received in revised form 27 March 2008
Accepted 2 April 2008
Available online 10 April 2008

Keywords:
Carcinogenicity
3D-QSAR
Docking
GRID
LBE
P450

ABSTRACT

A combination of 3D-QSAR, docking, local-binding energy (LBE) and GRID methods was applied as a tool to study and predict the mechanism of action of 100 carcinogenic benzene derivatives. Two 3D-QSAR models were obtained: (i) model of mouse carcinogenicity on the basis of 100 chemicals (model 1) and (ii) model of the differences in mouse and rat carcinogenicity on the basis of 73 compounds (model 2). 3D-QSAR regression maps indicated the important differences in species carcinogenicity, and the molecular positions associated with them. In order to evaluate the role of P450 metabolic process in carcinogenicity, the following approaches were used. The 3D models of CYP2E1 for mouse and rat were built up. A docking study was applied and the important ligand–protein residues interactions and oxidation positions of the molecules were identified. A new approach for quantitative assessment of metabolism pathways was developed, which enabled us to describe the species differences in CYP2E1 metabolism, and how it can be related to differences in the carcinogenic potential for a subset of compounds. The binding energies of the important substituents (local-binding energy—LBE) were calculated, in order to quantitatively demonstrate the contribution of the substituents in metabolic processes. Furthermore, a computational procedure was used for determining energetically favourable binding sites (GRID examination) of the enzymes. The GRID procedure allowed the identification of some important differences, related to species metabolism in CYP2E1. Comparing GRID, 3D-QSAR maps and LBE results, a similarity was identified, indicating a relationship between P450 metabolic processes and the differences in the carcinogenicity.

1. Introduction

Models to understand and predict the biological mechanism of carcinogenicity have used automated algorithms involving chemical descriptors [1], or rules including knowledge of DNA binding or metabolism (rule-based systems). Typical examples for rule-based software are expert systems, which use simple physico-chemical parameters, and work mainly on the assumption that toxicity is linked to the presence of toxic residues [2]. Some studies combine automated algorithms and rule-based methods [3]. However, these methods have limitations [4]. One of the obstacles lies in the generic characterization of processes explained by descriptors. For example, the energy of the lowest unoccupied molecular orbital (E_{LUMO}) is important for interaction with DNA [5] and for metabolism of carcinogenic compounds through P450 family [6]. P450 enzymes are responsible for 90% of phase I metabolism [7] and affect compounds within a defined range of E_{LUMO} values [8]. This divides the compounds, and means that success and interpretation of the models is possible within well-represented and defined classes.

Another important issue is the difference in chemical carcinogenicity in mouse, rat and other species [9]. A new approach implies direct interactions with DNA, where both toxicant and biological target molecules are involved in calculations [10]. This makes it possible to understand the reactive pathways and interpret results as biochemical processes. However, metabolic processes that can significantly change the primary chemicals into different metabolites have not been taken into account in Ref. [10].

The metabolic transformations of chemicals by P450 enzymes are important for toxicity [11], and can significantly reduce or increase the carcinogenic potential [12]. The activation of some chemicals to carcinogenic derivatives has been described previously [13]. Differences in xenobiotic oxidation in rat and mouse, and its relationship to carcinogenicity have been studied [14]. Compounds undergoing different oxidation tend to differ in toxicity [15]. Metabolic products formed by a ring hydroxylation are less toxic (i.e. oxidation provide an effective detoxication) than carbon, chlorine, nitro, amino and sulpho group reactions

* Corresponding author. Tel.: +39 045252477; fax: +39 045931585.
E-mail address: fratev@cbs.dtu.dk (F. Fratev).

1093-3263/$ – see front matter © 2008 Elsevier Inc. All rights reserved.
doi:10.1016/j.jmgm.2008.04.004

[16]. Hence, P450 metabolism as an important part of phase I metabolism, can have significant role in the interspecies differences in carcinogenicity.

It is important to know the main metabolic pathways. For instance, aflatoxin B1 has a well-defined oxidation mechanism via CYP1A2 and CYP3A4 [17,18]. Inhibiting one of these processes with natural or synthetic substances can reduce carcinogenicity [19]. The development of chemoprotective agents in many cases is based on detailed information about carcinogenic and toxicity activation processes through P450 members: CYP1A1 [20], CYP1A2 [21], CYP2E1 [22] and CYP3A4 [23].

The present study is focused on the differences in mouse and rat carcinogenicities and their relationships to P450 metabolism. The object of study is P450 enzyme CYP2E1. It is known that this enzyme is involved in metabolism of small benzene derivatives [24,25]. Experimental data shows differences in the metabolic products of these derivatives in mouse and rat [26]. Our aim is to analyze these differences and relate them to differences in metabolic mechanisms and chemical carcinogenic potential in the two species. We used a combination of 3D-QSAR, docking, LBE, and GRID analysis to model and detail these differences [27].

2. Methodology

2.1. Biological data

In many cases, carcinogenicity of a chemical is classified by activity. A numerical, continuous approach was introduced by Gold et al. [28]. Gold's database consists of standardized results, and for each chemical it reports the carcinogenicity in mouse and rat, using the parameter "Threshold dose 50" (TD_{50}), which is the dose rate that would give half the animals tumours within some standard experimental time—the "standard lifespan" for the species. The huge amount of information in Gold's database and the quantitative homogenous evaluation are two important advantages. This database has been therefore adopted as a basis for construction of the models presented in this article, and was used in other QSAR studies [1,29]. For each chemical the most potent TD_{50} was chosen. Original measurement units of TD_{50} were mg/kg of animal weight but in our study we used the following transformation:

$$\exp = \frac{\log(\mathrm{MW} \times 1000/\mathrm{TD}_{50})}{\log(\mathrm{MW}_{\mathrm{melphalan}} \times 1000/\mathrm{TD}_{50\,\mathrm{melphalan}})} \quad (1)$$

where exp is the transformed experimental value of TD_{50}, MW the molecular weight, $MW_{melphalan}$ and $TD_{50\ melphalan}$ are the molecular weight and TD_{50} of the most carcinogenic compound in our data set—Melphalan. This unit is better related to toxicity and carcinogenic potency [29]. Chem-X software [30] was used to calculate the molecular weight.

100 benzene analogues connected to mouse carcinogenicity were randomly selected, which comprise more than a 70% of the benzene derivatives compounds in the original database. For the remaining part of benzene derivatives, there were great variances in the original database that made it difficult to incorporate them in our model. In order to analyze the mouse carcinogenicity and its differences to rat carcinogenicity, two data sets were defined and two models were developed as follows.

First, a general data set consisting of all 100 compounds, which are presented in Tables 1 and 2 and 3S (supplementary material), was constructed. For these chemicals, only values for mouse carcinogenicity were used, and using 3D-QSAR approach, model 1 is built up. The compounds were divided in two sets: a training set, which was used for 3D-QSAR model development, and a test set, which was used to test the predictive ability of our models. The training set consisted of 81 compounds. The test set comprised 19 compounds, randomly selected from the primary set, which covered a wide range of carcinogenic data, and had the same structural differences as the training set.

Furthermore, to investigate the mouse and rat carcinogenicities and the difference between them, a second data set was constructed. Rat carcinogenicity data for 73 of all 100 compounds presented in model 1 were used and 3D-QSAR is applied just on these chemicals to build up model 2. This model was developed using respectively 49 and 24 compounds for the training and test set.

2.2. Model of molecules

Structures were collected and built up with fragments of the standard HyperChem library [31]. Conformational analysis was performed using molecular dynamics simulations under PM3 Hamiltonian in vacuum [32]. The compounds were heated for 2 ps to 700 K, and then were cooled for 5 ps to 300 K. Constant temperature was used during simulations. After 2 ps three low-energy conformers were selected, and after geometry optimization (PM3 method) with a high conjugate gradient criterion of 0.01 kcal mol^{-1} $Å^{-1}$, the lowest energy conformation was chosen.

2.3. 3D-QSAR method

Electrostatic and van der Waals (VdW) volume maps were generated for each compound, obtaining electrostatic potentials and VdW volume distributions in the different points of virtual grid. For these purposes the compounds were aligned and then map descriptors are calculated. The 3D-QSAR alignment and map descriptors calculations were performed by Chem-X software [30].

2.3.1. Alignment of molecules

The lowest energy conformers of the primary chemicals were chosen and aligned according to the main known binding feature of P450 and in particular CYP2E1. We based on crystallographic data for benzene derivatives in P450cam complexes [33,34] (during our study no crystallographic data for human CYP2C9 and rabbit CYP2B4 was available) and on previous docking modelling of compounds with similar substitution on benzene ring in the active sites of CYP1A2 [35,36], CYP2E1 [37,38] and CYP2A5 enzymes [39,40]. According to this data, all compounds were aligned over the common phenyl ring, and long chains of the ligands were overlapped in one direction. Alignment of aniline derivatives was made positioning amino groups in the place identical to aniline amino group position. For chemicals with only one reactive group (i.e. NH_2, NO_2, etc.), not presented in the long chains, we followed the same rule. The chemicals with many reactive groups and without long chains were randomly aligned. Rigid fitting was used at final alignment, based on least squares algorithm [41].

2.3.2. 3D-QSAR modelling

For steric map descriptors, we used the distribution of van der Waals volume around the compounds. As electrostatic descriptors, the electrostatic potentials that were generated with a positive dot charge unit were used. The grid had a density of one dot per 1 Å and was large enough to cover all the molecules. The value of energy cut-off was 20 kcal/mol. The standard deviations (S.D.s) of the electrostatic and steric fields were estimated. Electrostatic potentials gave a S.D. within the established range, as recommended in literature [42].

Statistical analysis was performed using the partial least square (PLS) method. The total number of steric and electrostatic descriptors was 3200. A cross-validation by "leave-one-out" was

applied to ten 3D-QSAR models for the training set, calculated with a number of components from 1 to 10, and the final optimum number of components is based on criterion of a minimum of standard error (E_{cross}). This procedure has been adopted in literature [43]. The cross-validation regression coefficient q^2 and the non-cross-validation coefficient r^2 were used to estimate the model qualities. Parameters q_s^2, q_e^2 and r_s^2, r_e^2 were related to the models with steric or electrostatic descriptors. To assess contribution of individual fields, a computation was performed of Q_s^2, Q_e^2 and Q^2, which are the regression coefficients, obtained from the cross-validation procedure applied respectively for all steric, electrostatic and total descriptors.

Predicted R^2_{pred} was used to estimate the predictive power of 3D-QSAR models:

$$R^2_{pred} = \frac{\text{S.D.} - \text{PRESS}}{\text{S.D.}} \quad (2)$$

where S.D. is the sum of standard deviation squares between the compound actual and predicted ligand activity, considering the training set; "PRESS" is the sum of S.D. for predicted and actual activity for each compound of the test set. Electrostatic and steric regions connected with carcinogenic potency on mouse, rat, and difference between these two species, were described by R^2-maps with appropriate level of importance.

2.4. Docking method

2.4.1. Homology modelling

The sequence of amino acid residues for mouse and rat CYP2E1 was taken from the Swiss-Prot/TrEMBL Protein Knowledgebase database (http://www.expasy.org) [44]. The homology models were constructed by ORFeus server (http://grdb.bioinfo.pl), using as template crystallographic data on CYP2C5 from the PDB databank [45] (pdb code: 1dt6). During our study no crystallographic data for human CYP2C9 and rabbit CYP2B4 was available (pdb code: 1og2, 1og5, 1po5 and 1suo)). ORFeus is a sensitive and fully automated sequence similarity search tool, available to the academic community via the Structure Prediction Meta Server (http://BioInfo.PL/Meta/) [46]. It is based on the alignment of two profiles, which include sequence information from the family of homologous proteins and predicted secondary structure. ORF-Blast is used to search for the initial family of proteins [47]. The generated homology models are presented in Table 4S (supplementary material). We adopt here the residues numbering according to the CYP2E1 sequence.

2.4.2. 3D-enzymes modelling

The 3D-enzymes models were constructed using MODELLER program [48]. The heme coordinates were directly transformed from crystallographic coordinates of 1dt6. The models correctness was checked for bad steric contacts. Amber 99 [49] molecular mechanics force field was used for optimization by conjugate gradient with level of 0.1 kcal mol^{-1} Å^{-1}. The centre of region, of benzene derivative ligands from crystallographic heme complex of P450cam, was adopted as a centre of the active site [37,38]. Molecular dynamic simulation was applied within 15 Å radius from the centre of the active site. The protein was heated to 500 K for 20 ps, and then cooled for 20 ps to 310 K. Constant temperature was used during simulations. The production run was 600 ps. After 500 ps a good equilibrium was reached and five minimum energy conformations were chosen (i.e. one for each 20 ps of the last 100 ps). After a new molecular mechanics optimization with a gradient criterion of 0.1 kcal mol^{-1} Å^{-1}, the enzyme conformation with lowest energy was chosen for further calculation. The heme was optimized individually by UHF PM3 method with gradient criterion of 0.1 kcal mol^{-1} Å^{-1}. For all heme atoms PM3 charges were used. We chose PM3 method instead of other semi empirical methods due to Fe parameterization.

2.4.3. Docking procedure

The docking study was carried out using AutoDock 3.0 program [50]. The grid was constructed with 40 points for each direction and density 0.2 Å. All compounds in docking study were optimized with PM3 method to conjugate gradient level of 0.01 kcal mol^{-1} Å^{-1} and then PM3 charges were applied for the docking calculations. In this way, both heme and ligands charges were calculated by the same method (PM3), which were used also in the compounds optimizations for 3D-QSAR. A Larmarckian genetic algorithm (LGA) was used to find the lowest energy docking poses. The number of individuals in population and maximum number of local search iterations were set to 50 and 300, respectively. Step sizes for changes the initial translation and quaternion were 0.2 and 5 Å. 100 independent runs to select the lowest-energy docking solution were used.

As an output, AutoDock gives total binding energies of the compounds as well as steric and electrostatic LBE for individual atoms. This information was used and the results were summarized for each atom (i.e. summarize the steric and electrostatic LBE). In this way, approximate values of atoms LBEs were obtained. The entropy effects were neglected in the present study.

2.5. GRID method

In order to investigate interaction between enzymes and benzene derivatives, a series of GRID [51] calculations were performed. The GRID program predicts non-covalent interactions between proteins with known three-dimensional structure and a small group as a probe representing the chemical features of a ligand. The calculations were done using version 21 of the GRID program. The box had as a centre the heme Fe atom, 26 Å × 26 Å × 26 Å dimensions, and density one point per 1 Å. As probes C_{sp^2}, DRY (hydrophobic), Csp^3, NH_2, aromatic amidine, aromatic amine and water were used. GRID maps were used to identify favoured binding sites of the enzymes.

3. Results

All models were checked for potential over-fitting with SIMCA software [52]. To check the validity and degree of over-fit for the models, the order of experimental values was randomly permuted 100 times and the separate models were fitted to all the permuted experimental values extracting as many components as was done with the original matrix. In this way we confirmed that all models were not over-fitted (see for example Fig. 1—supplementary material).

Fig. 1 presents 3D-QSAR model 1 test set results for mouse carcinogenicity. Tables 1 and 2 report experimental and calculated mouse and rat carcinogenicity values obtained from 3D-QSAR model 2 for the training and test set, respectively. Tables 1S, 2S and 3S (supplementary material) present the CAS numbers and not transformed carcinogenicity parameter TD_{50} for mouse and rat in mg/kg [28] for 3D-QSAR models 1 and 2, respectively. Statistics of all 3D-QSAR models are summarized in Table 3.

3.1. 3D-QSAR model for mouse carcinogenicity

The training set for mouse carcinogenicity (model 1) contains 81 ligands. A value of q^2 = 0.905 and error E_{cross} = 0.032, using eight components, were obtained via cross-validity procedure (leave-one-out). The same procedure, using all generated fields to assay

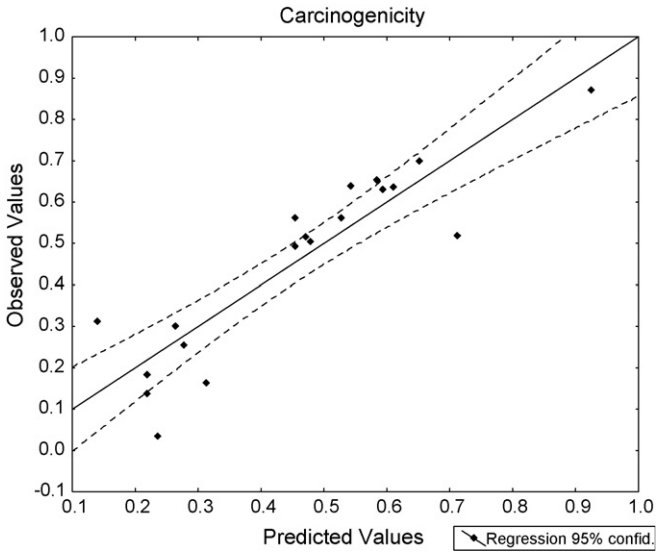

Fig. 1. Model 1 3D-QSAR results for the test set compounds.

the steric and electrostatic contribution, gave $Q^2 = 0.852$, $Q_e^2 = 0.550$ and $Q_s^2 = 0.72$. Comparison of electrostatic and steric models showed better predictive ability of steric fields, indicating higher contribution of these interactions. Combination of both fields gave better Q^2. The general model explained 98.4% of the total variation in the training set. The correlation was $r^2 = 0.952$.

3D-QSAR model 1 for mouse carcinogenicity had a good predictive ability as evident from results based on the test set (see Fig. 1 and Table 3). The predicted values were very close to the experimental ones and the correlation coefficient gave $R^2_{pred} = 0.87$ for 19 compounds. These results support the compounds alignment model. Model 2 based on 49 compounds was very similar to model 1. Additionally, all models with only steric or electrostatic field gave high q^2 and r^2 allowing a reliable assessment of the contributions of these interactions.

Figs. 2A and B (see supplementary material) present the regression-squared 3D-QSAR contour maps for mouse carcinogenicity using model 2. Regions with regression coefficient $R^2 = 0.05$ are coloured in blue, while regions with R^2 values in the range of 0.25–0.5 are in red.

3.2. 3D-QSAR model for rat carcinogenicity

3D-QSAR study on rat gave good results: $q^2 = 0.924$ and error $E_{cross} = 0.023$ using seven components. The correlation was $r^2 = 0.976$. The predictive ability of this model was evaluated with the test set and gave $R^2_{pred} = 0.65$.

The electrostatic and steric models had $Q_e^2 = 0.735$ and $Q_s^2 = 0.566$, respectively, which indicates that in this case electrostatic interactions were more important. Seven components, which covered 95.4% and 93.7% of carcinogenicity variations, were used for the conventional PLS models with steric and electrostatic fields, giving good predictive models.

Figs. 3A and B (see supplementary material) show rat 3D-QSAR electrostatic and steric R^2 contour maps defined as in Figs. 2A and B.

3.3. 3D-QSAR model for the difference in mouse and rat carcinogenicity

This study includes 49 ligands with TD_{50} values for both mouse and rat. PLS analysis gave a good $q^2 = 0.83$. Seven components were used and a value of $r^2 = 0.876$ was obtained. These values indicate the potential of this QSAR model for predicting the differences between mouse and rat carcinogenicity.

The information about individual steric and electrostatic models is presented in Table 3. The results illustrate a slightly higher electrostatic contribution, while combining results for both fields improved them significantly. Comparison of individual rat Q_s^2 and Q_e^2 values with those from mouse carcinogenicity model showed not only quantitative but also qualitative differences. This fact leads to the hypothesis that there are differences in rat and mouse ligand–receptor interactions linked to carcinogenicity. Figs. 2 and 3 present the R^2 contour maps for the differences in mouse and rat carcinogenicity; regions with squares of the regression coefficient $R^2 = 0.05$ are coloured in blue, while regions with R^2 values in range of 0.2–0.5 are coloured in red (range of 0.1–0.5 in Fig. 3).

3.4. Docking results

Seven aniline derivates and *N*,*N*′-dimethylaniline were selected for our docking study. These compounds had high differences in their mouse and rat carcinogenicity.

Fig. 4 presents the local binding energy (LBE) in kcal/mol for individual reactive atoms, and oxidation positions for selected chemicals in the active site of mouse and rat CYP2E1 enzymes. LBE results for positions related to other oxidation processes, which can produce different metabolites, are also presented. The results for all atoms showed that other metabolic pathways are less probable. Figs. 5 and 6 present the aniline position in the binding sites of mouse and rat CYP2E1 respectively, and the most important residues for the ligand–protein interaction. The atom nearest to the heme iron in mouse CYP2E1 is at para position, at a distance of 2.11 Å (H-Fe atom distance, no C-Fe distance was used). The lowest LBE was for the carbon atom at the same place, with a value of −0.99 kcal/mol. The orientation for *p*-hydroxylation agrees with previous docking models and experimental data for aniline metabolism [37,38]. Important interactions were identified with Ile115, Phe207, Phe298, Ala299, Thr303, Leu363, Val364 and Leu368. There is a π–π stacking between the phenyl ring of aniline and Phe298 and Phe207.

The oxidation position of aniline in CYP2E1 was at the same position in rat and mouse, but there were important differences between the species. The distance to iron was approximately twice in rat (3.85 Å) and the lowest LBE was at carbon in position one (see Fig. 4), thus not the nearest to the heme Fe atom. These differences arose because aniline amino group forms a strong H-bond with backbone oxygen of Gly479, which was far from the heme. There was also an additional contribution of Leu363 and Phe478 in this part of the enzyme. No interaction with Ile115 and π–π stacking with Phe298 was found. The reasons for different aniline binding in rat are linked to the large CYP2E1 conformational changes for some residues and especially in Phe298. Both 3D modelling and molecular dynamics simulation models gave the same results. The position of Phe298 ring in mouse was close to heme and increased the π–π stacking, but in rat the big difference (see Figs. 5–8) indicates the above-mentioned aniline binding. In addition, a rat Ala299 played a role as a barrier and prevented the formation of a strong aniline–heme complex.

The comparison with other species CYP2E1 3D models [37,38] shows that conformational changes are probably an important factor for aniline derivatives metabolism, but only in case of mouse CYP2E1 they lead to essential differences in aniline binding. These important changes lead to a larger energy contribution on ortho positions for most chemicals. The LBE differences between para and ortho positions for rat CYP2E1 were six times higher than those for mouse, which may explain why ortho metabolic

Table 1
3D-QSAR model 2 results for the training set compounds

Name[a]	Mouse			Rat			Difference		
	exp[b]	pred[c]	res[d]	exp	pred	res	exp	pred	res
1,2-Dichlorobenzene	0.339	0.352	−0.013	0.547	0.536	0.011	0.208	0.210	−0.002
1-Chloro-2,4-dinitrobenzene	0.499	0.464	0.035	0.663	0.667	−0.004	0.164	0.189	−0.025
2,4,5-Trichlorophenoxyacetic acid	0.587	0.605	−0.018	0.690	0.683	0.007	0.103	0.091	0.012
2,4-Diaminoanisole sulfate	0.434	0.446	−0.012	0.516	0.527	−0.011	0.082	0.076	0.006
2,5-Xylidine	0.374	0.343	0.031	0.456	0.447	0.009	0.082	0.096	−0.014
2,6-Dichloro-*p*-phenylenediamine	0.367	0.398	−0.031	0.360	0.410	−0.050	−0.007	−0.015	0.008
2-Amino-4-nitrophenol	0.365	0.404	−0.039	0.528	0.527	0.001	0.163	0.102	0.061
2-Amino-5-nitrophenol	0.228	0.256	−0.028	0.587	0.596	−0.009	0.359	0.335	0.024
2-Chloro-*p*-phenylenediamine	0.319	0.345	−0.026	0.435	0.412	0.023	0.116	0.071	0.045
2-Nitro-*p*-phenylenediamine	0.382	0.308	0.074	0.446	0.455	−0.009	0.064	0.099	−0.035
3-(3,4-Dichlorophenyl)-1,1-dimethylurea	0.413	0.414	−0.001	0.541	0.547	−0.006	0.128	0.148	−0.020
3-(*p*-Chlorophenyl)-1,1-dimethylurea	0.428	0.410	0.018	0.529	0.519	0.010	0.101	0.119	−0.018
3-Amino-9-ethylcarbazole	0.601	0.596	0.005	0.604	0.608	−0.004	0.003	0.038	−0.035
3-Chloro-*p*-toluidine	0.296	0.320	−0.024	0.400	0.412	−0.012	0.104	0.089	0.015
3-Nitro-*p*-acetophenetide	0.318	0.337	−0.019	0.244	0.252	−0.008	−0.074	−0.083	0.009
4-(2-Chloroacetyl)acetanilide	0.264	0.277	−0.013	0.443	0.453	−0.010	0.179	0.201	−0.022
4-Chloro-*m*-phenylenediamine	0.330	0.295	0.035	0.458	0.439	0.019	0.128	0.152	−0.024
4-Chloro-*o*-phenylenediamine	0.317	0.328	−0.011	0.450	0.451	−0.001	0.133	0.131	0.002
5-Chloro-*o*-toluidine	0.478	0.443	0.035	0.361	0.374	−0.013	−0.117	−0.128	0.011
5-Nitro-*o*-anisidine	0.296	0.362	−0.066	0.595	0.586	0.009	0.299	0.239	0.060
5-Nitro-*o*-toluidine	0.447	0.472	−0.025	0.589	0.579	0.010	0.142	0.113	0.029
Aniline	0.150	0.279	−0.129	0.476	0.472	0.004	0.326	0.247	0.079
Benzaldehyde	0.304	0.305	−0.001	0.476	0.490	−0.014	0.172	0.188	−0.016
Benzyl acetate	0.309	0.297	0.012	0.429	0.444	−0.015	0.120	0.129	−0.009
Benzyl chloride	0.510	0.468	0.042	0.550	0.551	−0.001	0.040	0.065	−0.025
Butylated hydroxytoluene	0.397	0.422	−0.025	0.402	0.389	0.013	0.005	−0.037	0.042
Caffeic acid	0.253	0.225	0.028	0.438	0.442	−0.004	0.185	0.237	−0.052
Chlorobenzene	0.396	0.370	0.026	0.419	0.469	−0.050	0.023	0.080	−0.057
Di (2-ethylhexyl)phthalate	0.427	0.429	−0.002	0.400	0.405	−0.005	−0.027	−0.026	−0.001
Fluometuron	0.441	0.447	−0.006	0.465	0.449	0.016	0.024	0.009	0.015
Gemfibrozil	0.487	0.496	−0.009	0.414	0.416	−0.002	−0.073	−0.094	0.021
HC blue no. 2	0.133	0.109	0.024	0.339	0.333	0.006	0.206	0.218	−0.012
Hydroquinone	0.515	0.403	0.112	0.508	0.493	0.015	−0.007	0.062	−0.069
m-Cresidine	0.450	0.422	0.028	0.388	0.428	−0.040	−0.062	−0.041	−0.021
m-Toluidine	0.164	0.206	−0.042	0.416	0.451	−0.035	0.252	0.239	0.013
Melphalan	1.000	1.011	−0.011	1.000	0.997	0.003	0.000	0.012	−0.012
o-Nitroanisole	0.479	0.497	−0.018	0.641	0.662	−0.021	0.162	0.175	−0.013
o-Toluidine	0.344	0.345	−0.001	0.494	0.470	0.024	0.150	0.135	0.015
Oxprenolol	0.446	0.430	0.016	0.339	0.323	0.016	−0.107	−0.097	−0.010
p-Chloroaniline	0.280	0.300	−0.020	0.499	0.457	0.042	0.219	0.175	0.044
p-Cresidine	0.518	0.508	0.010	0.503	0.513	−0.010	−0.015	−0.014	−0.001
p-Nitroaniline	0.391	0.377	0.014	0.546	0.567	−0.021	0.155	0.171	−0.016
Pentachloronitrobenzene	0.395	0.336	0.059	0.538	0.512	0.026	0.143	0.139	0.004
Phenacetin	0.526	0.451	0.075	0.513	0.529	−0.016	−0.013	0.056	−0.069
Phenylephrine	0.361	0.304	0.057	0.439	0.405	0.034	0.078	0.096	−0.018
Procarbazine	0.966	0.966	0.000	0.927	0.922	0.005	−0.039	−0.050	0.011
Styrene	0.329	0.365	−0.036	0.513	0.456	0.057	0.184	0.099	0.085
Trifluralin	0.479	0.474	0.005	0.426	0.422	0.004	−0.053	−0.034	−0.019
Zearalenone	0.660	0.642	0.018	0.623	0.620	0.003	−0.037	−0.043	0.006

[a] Chemical names.
[b] Experimental carcinogenicity, see in the text.
[c] Predicted by 3D-QSAR model 2 carcinogenicity.
[d] Differences between experimental and predicted (rat minus mouse data) by 3D-QSAR model 2.

production in rat was eight times more abundant than in mouse [26].

Our results show that para position of aniline is closest to the heme in mouse, leading to better detoxication and lower carcinogenic potential, in agreement with experimental data (see Table 1); π–π stacking with Phe298 favours this process. Instead, for rat the interacting part is far from heme, thus reducing aniline transport to heme and detoxication.

Furthermore, binding features such as oxidation position and carcinogenic potential on 3-chloro-*p*-toluidine, 4-chloro-*o*-toluidine, *m*-toluidine, *o*-toluidine and *N*,*N*′-dimethylaniline in the active site of CYP2E1 were studied. 4-Chloro-*o*-toluidine and *N*,*N*′-dimethylaniline undergo CYP2 metabolism [53–55]. For the remaining chemicals experimental data about P450 metabolism was not available, but general metabolic pathways and products for *m*-toluidine and *o*-toluidine are known [56]. The chemical structure of these compounds [37,38] lead to the assumption about CYP2E1 metabolism that is discussed below.

The results for 3-chloro-*p*-toluidine show a hydroxylation at position 6 of the ring for both rat and mouse CYP2E1 enzymes. The distance to iron was 3.78 Å for rat and 1.59 Å for mouse. In mouse the LBE was lower than in rat (see Fig. 4). In rat the interaction of the methyl group with Ile115 contributed to an unfavourable amino orientation for the H-bond with backbone oxygen Gly479. For both mouse and rat there is a large difference between ring and methyl carbon LBE values, which may indicate better detoxication and consequently lower carcinogenicity. However, according to the distances and LBE values, the hydroxylation is more evident in mouse, and this is a possible explanation for the lower carcinogenicity (see Table 1).

Table 2
3D-QSAR Model 2 results for the test set compounds

Name[a]	Mouse			Rat			Difference		
	exp[b]	pred[c]	res[d]	exp	pred	res	exp	pred	res
1*H*-Benzotriazole	0.237	0.290	−0.053	0.258	0.361	−0.103	0.021	−0.019	0.040
2,4,5-Trimethylaniline	0.544	0.520	0.024	0.602	0.605	−0.003	0.058	0.009	0.049
2,4,6-Trichlorophenol	0.343	0.363	−0.020	0.337	0.472	−0.135	−0.006	−0.119	0.113
2,4,6-Trimethylaniline	0.573	0.555	0.018	0.694	0.602	0.092	0.121	0.179	−0.058
2,4-Diaminotoluene	0.442	0.474	−0.032	0.685	0.611	0.074	0.243	0.295	−0.052
2,4-Xylidine	0.637	0.526	0.111	0.420	0.567	−0.147	−0.217	−0.420	0.203
3-(Chloromethyl)pyridine hydrochloride	0.401	0.409	−0.008	0.389	0.499	−0.110	−0.012	−0.085	0.073
4-Chloro-*o*-toluidine	0.631	0.505	0.126	0.376	0.476	−0.100	−0.255	−0.433	0.178
4-Nitroanthranilic acid	0.185	0.167	0.018	0.188	0.350	−0.162	0.003	−0.084	0.087
8-Hidroxyquinoline	0.359	0.405	−0.046	0.245	0.389	−0.144	−0.114	−0.228	0.114
Benzyl alcohol	0.034	0.247	−0.213	0.302	0.398	−0.096	0.268	0.354	−0.086
Chloramben	0.254	0.396	−0.142	0.288	0.433	−0.145	0.034	−0.041	0.075
Diallyl phthalate	0.312	0.323	−0.011	0.512	0.590	−0.078	0.200	0.106	0.094
Hexachlorobenzene	0.605	0.583	0.022	0.661	0.641	0.020	0.056	0.016	0.040
Isoniazid	0.652	0.471	0.181	0.481	0.497	−0.016	−0.171	−0.313	0.142
m-Phenylenediamine	0.296	0.412	−0.116	0.285	0.470	−0.185	−0.011	−0.095	0.084
N,*N*′-dimethylaniline	0.492	0.432	0.060	0.470	0.517	−0.047	−0.022	−0.088	0.066
Nicotinic acid	0.779	0.730	0.049	0.838	0.759	0.079	0.059	0.003	0.056
o-Phenylenediamine	0.499	0.450	0.049	0.703	0.626	0.077	0.204	0.213	−0.009
p-Phenylenediamine	0.225	0.206	0.019	0.291	0.410	−0.119	0.066	0.021	0.045
Propyl gallate	0.225	0.215	0.010	0.385	0.456	−0.071	0.160	0.192	−0.032
Resorcinol	0.761	0.547	0.214	0.425	0.477	−0.052	−0.336	−0.569	0.233
Sotalol	0.302	0.310	−0.008	0.210	0.353	−0.143	−0.092	−0.186	0.094
Toluene	0.227	0.355	−0.128	0.160	0.426	−0.266	−0.067	−0.169	0.102

[a,b,c,d]See the relative marks in Table 1.

4-Chloro-*o*-toluidine metabolism through mouse CYP2E1 gave demethylation with Fe at a distance of 1.11 Å with the hydrogen of the methyl group, and LBE on methyl carbon atom is −0.92 kcal/mol. For rat CYP2E1, a hydroxylation via position three was the main mechanism. These results can explain the higher mouse toxicity linked to the oxidation pathway and reflected in the final carcinogenicity.

Position 4 is nearest to the iron heme atom in case of *m*-toluidine, at a distance of 3.77 Å in the active site of rat CYP2E1. There is strong H binding between the amino group and the backbone oxygen of Gly479. These results are very similar to those for aniline in the same enzyme. Both chemicals underwent *p*-hydroxylation with similar LBE values, indicating equal toxic potential and similar rat carcinogenicity (see Table 1). As in the case of rat CYP2E1 aniline complex, the LBE values for ortho and para positions were similar, and there was a significant ortho energy contribution. This can explain the experimentally equal range of para and ortho metabolites [56] and the higher carcinogenicity in rat than in mouse. The distance to the Fe atom and LBE values of mouse enzyme were respectively 1.85 Å and −0.97 kcal/mol, which are close to the aniline values for mouse. In mouse the hydroxylation position of *m*-toluidine is 5, and our LBE values indicate a similar metabolism and possible carcinogenicity for mouse and rat.

The same conclusion is reached considering the results for metabolism on *o*-toluidine. The metabolic pathway is oxidation in para position for both species, differing only in LBE values. The expected similar range of metabolism and carcinogenic effect is supported by the experimental carcinogenicity. The predicted ring *p*-hydroxylation is in agreement with the experimental data [56].

Docking results for *N*,*N*′-dimethylaniline show *N*-demethylation, in agreement with experimental studies [55] and similar binding features for both species, indicating an equal P450 toxic potential for mouse and rat. LBE value of methyl carbon atom was much lower than those of carbons in all ring positions (in Fig. 4 we only show the lowest ring carbon LBE value), which excludes ring oxidation mechanism.

Other examples for compounds with a high species differences in carcinogenicity are 2,4-xylidine and 2,5-xylidine. 2,4-Xylidine and 2,6-xylidine undergo CYP2E1 metabolism [57], while the P450 related activity of the 2,5-xylidine is apparently unknown. Figs. 7 and 8 present the docking views of 2,4-xylidine in the active site of mouse and rat CYP2E1. The compound underwent demethylation in mouse via position 4 and ring oxidation in rat via positions 5. The distances to iron were 3.92 and 1.82 Å in rat and mouseCYP2E1, respectively. 2,5-Xylidine did not show oxidation path differences, and had similar LBE values and carcinogenicity in both species. Conversely, 2,4-xylidine, which may cause direct DNA damage [58], underwent demethylation at mouse CYP2E1 similar to 4-chloro-*o*-toluidine, and the carcinogenicity is similar.

Table 3
Summarized statistical results of models 1 and 2

	Model 1	Model 2		
	Mouse	Mouse	Rat	Difference
NC[a]	81	49	49	49
q^{2}[b]	0.91	0.89	0.93	0.83
r^2	0.95	0.94	0.98	0.91
F	332.4	94.2	235.8	57.0
OC	8	7	7	7
Q^{2}[c]	0.85	0.82	0.81	0.60
Q_s^2	0.72	0.70	0.57	0.39
Q_e^2	0.55	0.63	0.74	0.45
R^2_{pred}[d]	0.87	0.76	0.65	0.64
n	19	24	24	24

[a] Number of the compounds in 3D-QSAR model.
[b] q^2, r^2, *F*, OC are cross-validation regression coefficient, regression coefficient, Fisher criterion and optimum number of components.
[c] Q^2, Q_s^2, Q_e^2 are cross-validation regression coefficient for the total number of descriptors, steric and electrostatic, respectively.
[d] R^2_{pred} and *n* are predictive regression coefficient only for the test set compounds and number of the compounds in the test set.

3.5. GRID results

Figs. 9 and 10 present GRID maps of the favoured binding sites of mouse and rat CYP2E1 at the binding energy level of −3 kcal/

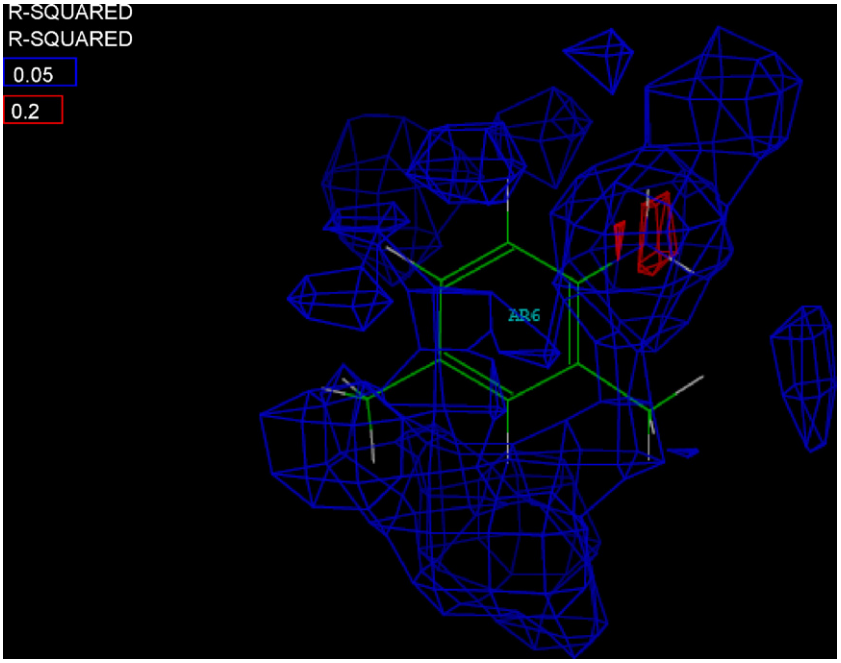

Fig. 2. 3D-QSAR mouse and rat differences carcinogenicity regression electrostatic contour map using 2,4-xylidine for visualization. Regions with values of the regression coefficient squared (R^2) equal to 0.05 are coloured in blue, while regions with R^2 values in the range of 0.2–0.5 in red.

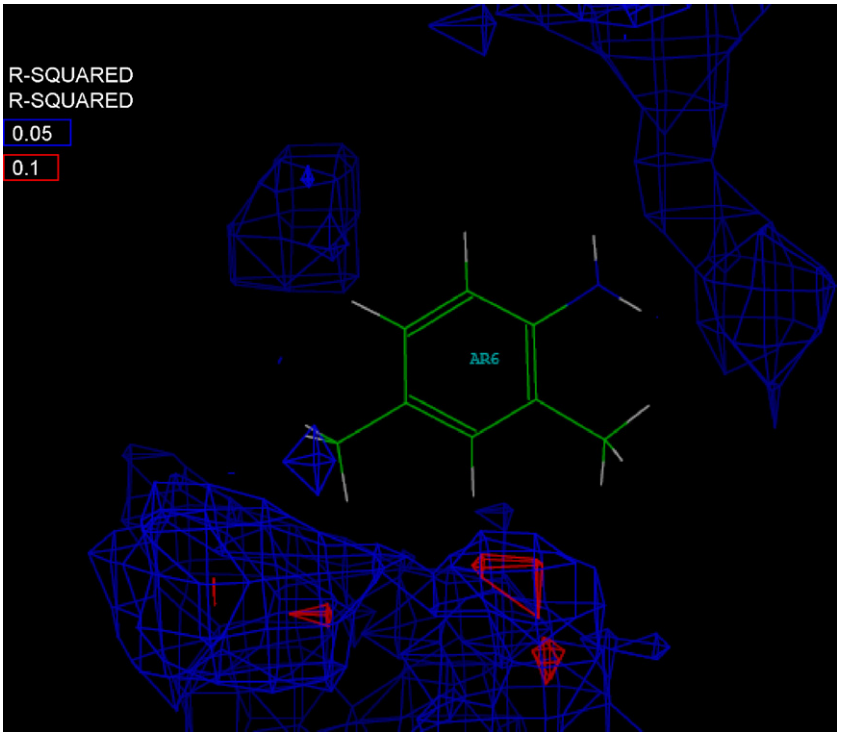

Fig. 3. 3D-QSAR mouse and rat differences carcinogenicity regression steric contour map using 2,4-xylidine for visualization. Regions with values of the regression coefficient squared (R^2) equal to 0.05 are coloured in blue, while regions with R^2 values in the range of 0.1–0.5 in red.

mol, using C_{sp^2} as a probe atom. For visualization we used the 2,4-xylidine coordinates obtained in docking analysis. Figs. 9 and 10 show the magnified regions near to this chemical. There were three CYP2E1 energy minima for mouse, close to the heme. The lowest minimum was around the para methyl group of 2,4-xylidine. In the region around Phe298 and Phe207 there were also possible binding positions (see the left top in Fig. 9 and also Figs. 5–8). The heme part was more accessible for mouse CYP2E1 than for rat. There was no favoured binding site around Phe298 in rat enzyme, but the binding pocket close to Phe207 was prominent. Both the GRID and docking methods identified this difference. At the level −1.4 kcal/mol all docking positions overlapped with the favoured binding regions in GRID maps, which indicated a good agreement between docking and GRID results.

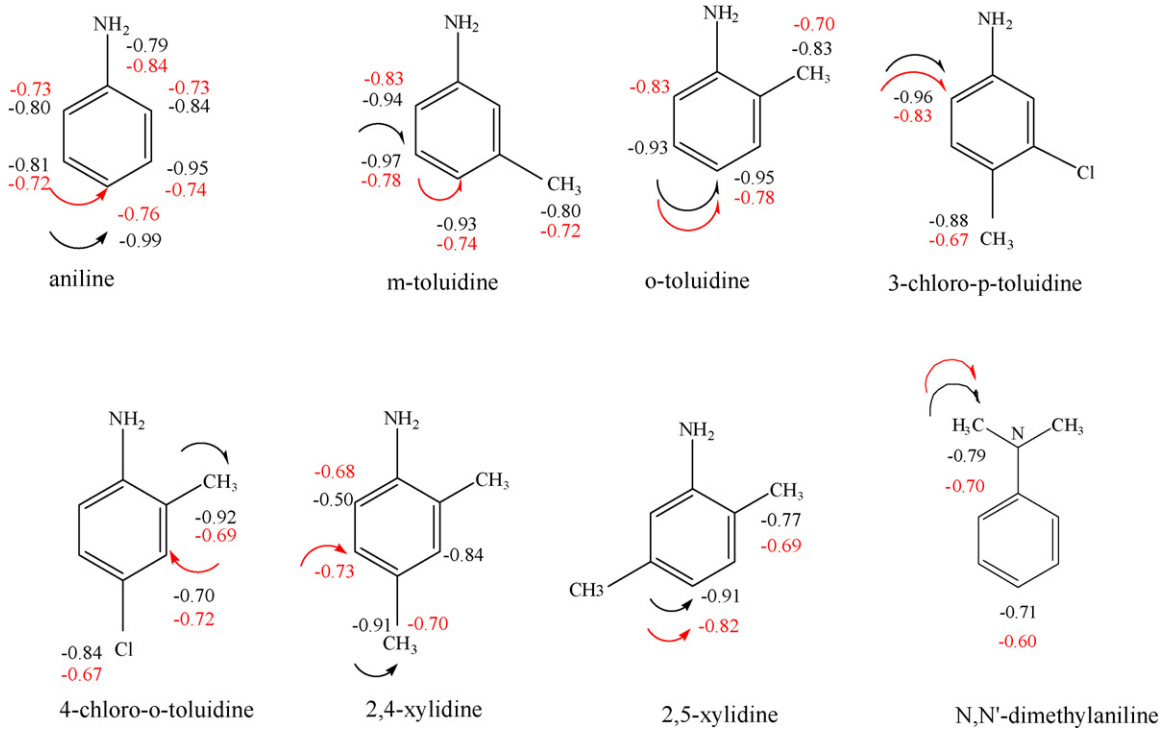

Fig. 4. Oxidation positions indicated and lowest LBE values (kcal/mol) by arrows for aniline derivatives. In black and red are marked the values for mouse and rat, respectively.

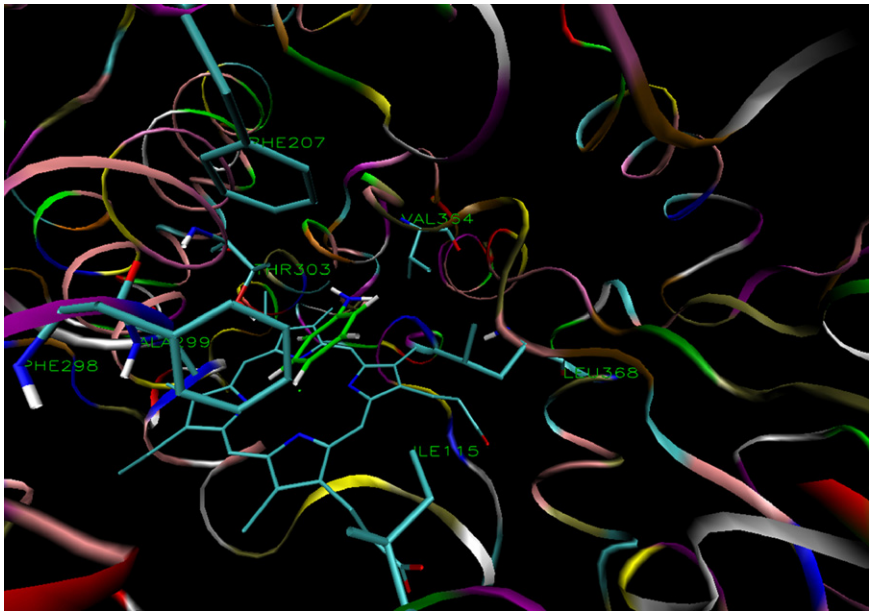

Fig. 5. Docking view of aniline in the binding site of the CYP2E1 mouse enzyme.

Using NH_2, aromatic amide and aromatic amine as a probe, the GRID calculations highlighted an important feature of the CYP2E1 family: in benzene derivatives chemicals with one amino group, this group probably cannot interact directly with the Fe heme atom, but diamino compounds can. There was also a favoured binding region around Phe207, which is an indication that this site is important not only for aromatic (C_{sp^2} probe), but for other classes of compounds too and probably forms a second binding site. GRID results identified a favoured binding site at a distance of 10 Å from heme. Recent crystallographic data for the human complex warfarin-CYP2C9 enzyme located a new binding pocket in the same region, which supports our result and suggests that P450 may simultaneously accommodate multiple ligands during its biological function [59].

3.6. Species-related differences in carcinogenicity indicated by 3D-QSAR and docking approaches

3.6.1. A difference between mouse and rat carcinogenicity indicated by 3D-QSAR maps

The aim of this study is to obtain information about differences in mouse and rat carcinogenicity. Contour maps (Figs. 2 and 3, 2A–

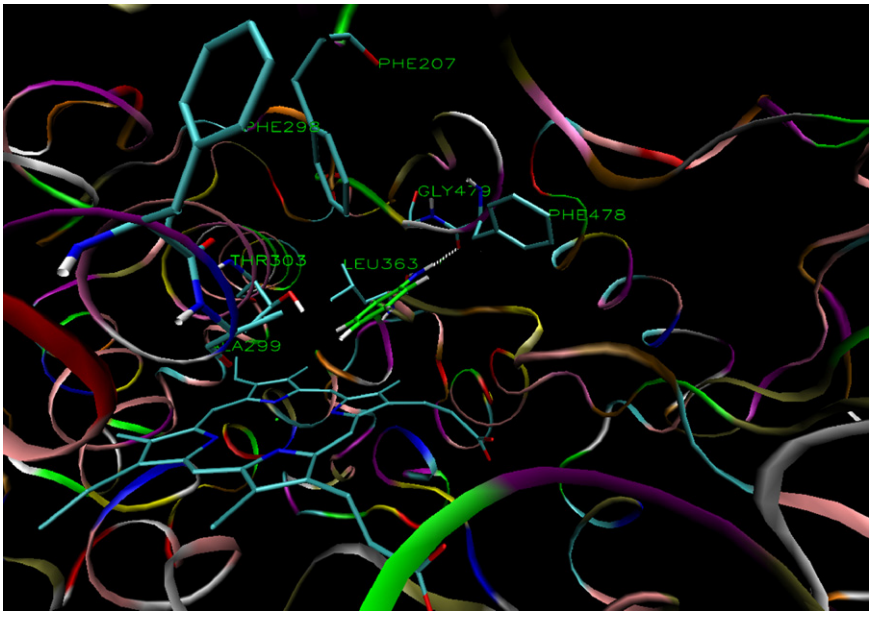

Fig. 6. Docking view of aniline in the binding site of the CYP2E1 rat enzyme. With white dotted line is marked H bound between aniline and GLY479.

3A and 2B–3B) from 3D-QSAR investigation were used to compare the regions and substituents important for the differences in carcinogenicity. There were no essential differences between 3D-QSAR maps from mouse model 1 and smaller model 2 and we focus here only on the maps derived from model 2. 2,4-Xylidine is used to visualize compound regions significant for carcinogenicity.

Figs. 2A and 3A (see supplementary material) present mouse and rat electrostatic 3D-QSAR regression maps. One of the most significant regions ($0.25 \leq R^2 \leq 0.5$) at position 5 of the aromatic ring was similar for both species. However, for rat the second significant region was between positions 5 and 6, while for mouse it was in position 4. There was a difference in position 3 due to the higher significance of the chemical groups in rat. In addition, positions 1 and 2 contributed more for rat carcinogenicity.

The mouse and rat steric 3D-QSAR regression maps (Figs. 2B and 3B (see supplementary material)) indicate differences similar to the electrostatic ones. In rat position 3, the regions at position 1 (especially in the top left region in Fig. 3B) and position 5 were with higher contribution to carcinogenicity than in mouse. The blue contour in ortho position for rat indicates a big region in the receptor where ligands interact. Para regions, contrary to mouse, had no carcinogenicity contribution or are less significant for rat.

The most important information about species-related differences can be obtained from maps derived from 3D-QSAR model for differences between mouse and rat carcinogenicity (Figs. 2 and 3). The red region in Fig. 2 indicates that electrostatic differences between rat and mouse carcinogenicity comes mainly from the different electrostatic interaction of the amino group and the other

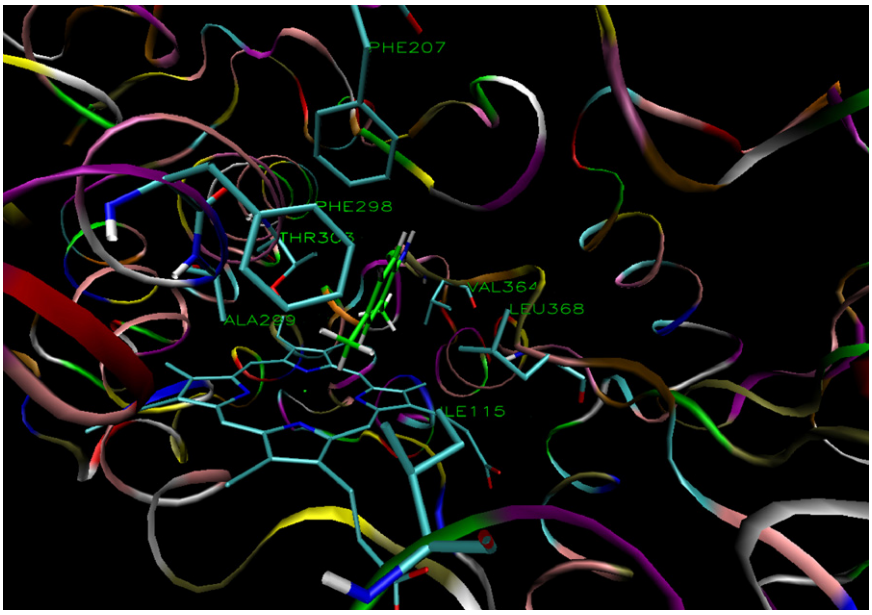

Fig. 7. Docking view of 2,4-xylidine in the binding site of the CYP2E1 mouse enzyme.

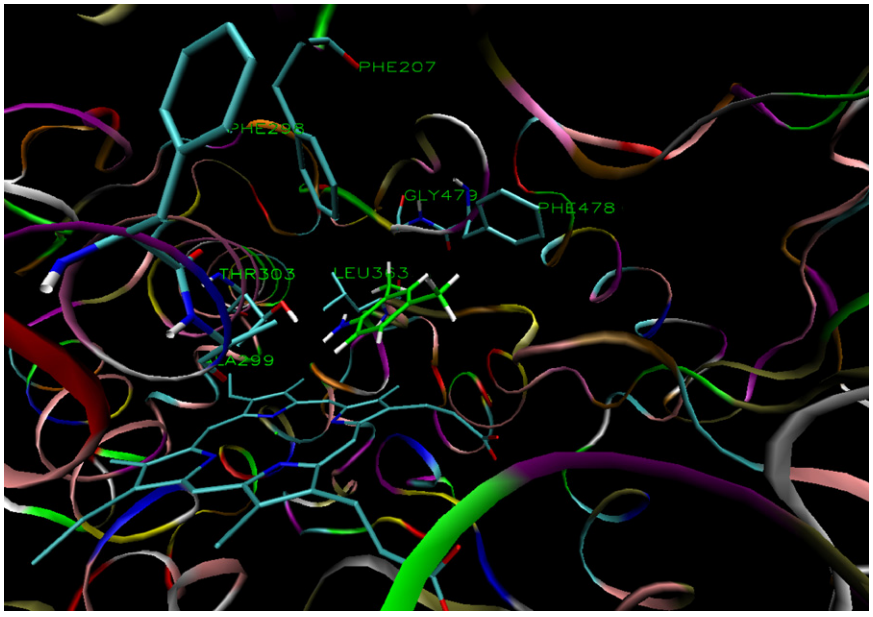

Fig. 8. Docking view of 2,4-xylidine in the binding site of the CYP2E1 rat enzyme.

substituents in position 1. The steric map (Fig. 3) indicates other important carcinogenicity differences mentioned above: the significance of substituents' interaction in para position, and in position 1.

3.6.2. A difference between mouse and rat carcinogenicity indicated by docking LBE values

LBE results were analyzed to see how metabolic processes contribute to differences in carcinogenicity. The LBE and oxidation positions in mouse and rat CYP2E1 are presented in Fig. 4. As shown in the docking paragraph, LBE can indicate quantitatively the likely metabolic pathway, which leads to differences in chemical oxidation mechanism and carcinogenic potential. A similar conclusion can be done considering only the orientation of the compounds to the iron atom (i.e. qualitative indication of the oxidation position). However, when one chemical shows in both mouse and rat identical metabolism, the only way to describe the differences can be quantitative, using some appropriate descriptor. LBE is a descriptor that can be linked to differences in the rate of metabolism indicating differences in carcinogenic potential. The lower values of LBE on chemicals oxidation positions corresponded to more favourable binding and consequently to better rate of oxidation. Following this hypothesis we calculated the differences between rat and mouse LBE (ΔLBE) for the oxidation positions of aniline, 3-chloro-*p*-toluidine, *o*-toluidine and 2,5-xylidine, which underwent the same oxidation for both mouse and rat, according to our docking results (see Fig. 4). As a result, the ΔLBE values gave a good correlation with the differences between rat and mouse carcinogenicity (ΔCancer): $r = 0.95$, $F = 19.8$, $\alpha = 0.05$, S.E. = 0.03, $n = 4$, where parameter α presents the level of significance of the obtained regression and S.E. is the standard error. The compound with highest ΔLBE was aniline, showing the highest differences between rat and mouse carcinogenicity. All these compounds had a lower LBE in oxidation positions for mouse than for rat, and according to our hypothesis, indicated better detoxication and

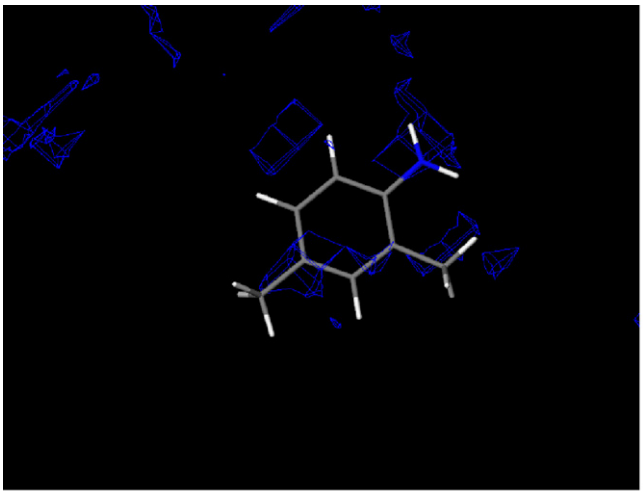

Fig. 9. GRID map for the favoured binding regions (−3.0 kcal/mol) in active site of the mouse CYP2E1 using C_{sp^2} atom as probe and 2,4-xylidine for visualization.

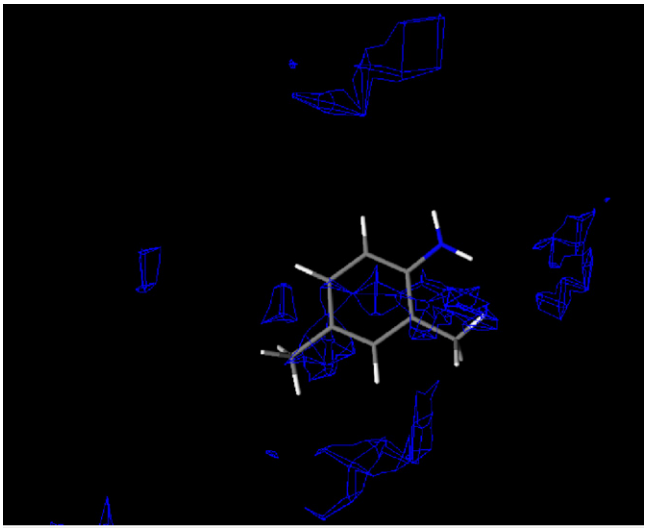

Fig. 10. GRID map for the favoured binding regions (−3.0 kcal/mol) in active site of the rat CYP2E1 using C_{sp^2} atom as probe and 2,4-xylidine for visualization.

hence lower carcinogenic potential. This result is supported by the experimental ΔCancer values, which are positive for all these chemicals (see Tables 1 and 2, column 10). Furthermore, we included compounds with different oxidation mechanism (i.e. all chemicals in Fig. 4) and applied the approach used above. 4-Chloro-toluidine, *N*,*N*′-dimethylaniline, *m*-toluidine and 2,4-xylidine showed higher rat carcinogenicity than mouse and for these four chemicals the value of ΔCancer changes its sign to minus (except *m*-toluidine). The module of ΔCancer was used and we found again a significant regression toward ΔLBE values: $r = 0.96$, $F = 77.27$, $\alpha < 0.01$, S.E. = 0.03, $n = 8$. From these results it can be concluded that the module of ΔCancer is related to ΔLBE. The compounds with higher ΔLBE gave higher ΔCancer. Hence, ΔLBE value can describe not only single oxidation mechanism, but it can be used as a general descriptor. The module of ΔCancer was used in order to avoid the influence of specific oxidation mechanisms, taking into account only the amount of the carcinogenicity differences. In other words, the quantity ΔLBE characterizes the value of species-related differences in carcinogenicity. However, absolute carcinogenic potential depends on the nature of oxidation mechanism. In our subset of aniline derivatives 4-chloro-toluidine and 2,4-xylidine show higher carcinogenicity for mouse than for rat due to demethylation, which can produce metabolites with higher carcinogenic potential compared to hydroxylation.

The results presented in this paragraph can be interpreted as a strong indication that there is a relationship between CYP2E1 metabolic process and differences between rat and mouse carcinogenicity of aniline derivatives.

3.7. Carcinogenicity relationships with the oxidations positions LBE values

We used the above-mentioned differences in LBE values in the binding site of CYP2E1 to explain the differences in mouse and rat carcinogenicity for a set of aniline derivatives. To study the contribution of CYP2E1 to carcinogenicity (i.e. not only the differences in carcinogenicity) we searched for all possible correlations to oxidations positions LBE values. Fig. 4 shows the LBE values included in our calculation. A moderate regression between mouse LBE values for the obtained oxidation positions and carcinogenicity was found: $r = 0.60$, $F = 3.30$, $\alpha = 0.12$, S.D. = 0.16, $n = 8$. *N*,*N*′-Dimethylaniline was a strong outlier and without this compound the following regression was obtained: $r = 0.86$, $F = 14.15$, $\alpha < 0.01$, S.D. = 0.11, $n = 7$; there was no correlation in the case of rat carcinogenicity.

3.8. 3D-QSAR, LBE and GRID comparisons

3.8.1. 3D-QSAR and LBE comparison

To study the contribution of CYP2E1 metabolism in carcinogenicity for all benzene derivatives in our data set, a combination of the results derived by 3D-QSAR and LBE methods was used.

3D-QSAR contour maps show regression values toward carcinogenicity of the ligands, and consequently the substituents involved in carcinogenicity process. Thus, comparison of 3D-QSAR significant maps regions with the same ones from LBE regression made it possible to study the mechanism of action and to compare the two approaches. Since there was a good agreement between these two methods using the LBE values for our subset of aniline derivatives, we consider it as a good indication that CYP2E1 contributed to carcinogenicity.

Using LBE values only at position 4 in mouse and without *N*,*N*′-dimethylaniline, the following regression was obtained: $r = 0.68$, $F = 4.20$, $\alpha = 0.10$, S.E. = 0.16, $n = 7$. For other positions in mouse, and all in rat, no correlation with carcinogenicity was found. Although the level of significance at position 4 in mouse was not high in LBE regression, it was similar to the mouse 3D-QSAR maps regression values on para position. Regression values between LBE and mouse carcinogenicity and those on the same position from 3D-QSAR maps were comparable. This fact independently supports the results from the previous paragraph and indicates that the CYP2E1 carcinogenicity relation could be extended for other chemicals in our data set of benzene derivatives.

3.8.2. 3D-QSAR and GRID maps comparison

3D-QSAR and GRID maps were compared. The GRID maps visualize the binding site of the enzymes at defined binding energy levels, calculated with different probe atoms (C_{sp^2} as an aromatic atom probe here). Hence, the GRID maps help locating positions of the lower LBE regions in the enzymes. One of the docked compounds (2,4-xylidine) was used to obtain information and visualize where in 3D-space these positions surround the chemicals and its substituents. This enabled us to combine docking and GRID results and to compare the same regions derived from 3D-QSAR regression maps. In the case of rat 2,4-xylidine position, which differs to those in mouse (see Figs. 7 and 8), we used one of the higher binding energy docking conformations (with an orientation for oxidation in para position) to have an equal mouse and rat GRID maps visualization. The difference in benzene ring centre coordinates was insignificant compared to the lower docking conformer. Similarly to the LBE-3D-QSAR comparison above, we assume here that, if there is good agreement between GRID lower energy sites in the enzymes and 3D-QSAR high regression regions, CYP2E1 contributed to carcinogenicity.

The most notable overlap between 3D-QSAR and GRID maps was found when rat GRID map and 3D-QSAR for the differences in carcinogenicity steric map were compared (see Figs. 3 and 10). The three most important regions indicated by 3D-QSAR map are presented in GRID map too: para position in benzene ring, position 3 and an important distant region in position 6 that probably is linked to the higher Phe207 rat binding energy contribution.

The comparisons of Figs. 2 and 3, 2A–B, 3A–B (see supplementary material) and 9 and 10 show that there is another similarity. One of the favoured CYP2E1 binding regions close to the heme part (in the figures para position on 2,4-xylidine) was in position 4 on the benzene ring as in the 3D-QSAR maps. The ortho position in rat 3D-QSAR maps and GRID map was more accessible than in mouse ones. The low energy region in position 3 in rat GRID CYP2E1 map is in good agreement to 3D-QSAR rat electrostatic and steric maps.

Only the steric probe was used in our GRID calculation (C_{sp^2} atom), which can explain why only the steric 3D-QSAR map correlated to GRID map. The differences in carcinogenicity identified by the docking analysis mainly come from differences in residue positions and interactions with rat CYP2E1 enzyme.

These results show that there is a good match between GRID rat map and 3D-QSAR steric map for the differences in carcinogenicity; the lower energy binding regions in CYP2E1 fit well with those significant for differences in carcinogenicity, indicating their relationship. The comparison between other maps linked to carcinogenicity shows less notable similarities. We can conclude that for an essential part of the benzene derivatives studied here, CYP2E1 is a likely biological target that could explain the species-related differences in carcinogenicity. However, as in the case of LBE results above, we were not able to find a strong relationship between carcinogenicity and P450 metabolism.

4. Discussion

3D-QSAR results indicate a similarity in mechanisms of carcinogenicity, but differences in species receptors. Based on

3D-QSAR maps and docking results we can offer qualitative explanations for these differences, due to species features of the P450 member CYP2E1, that account for the differences in oxidation positions and carcinogenic potential on the metabolites; 3D-QSAR maps indicate that in rat there was a higher contribution related to the ortho residues, while in mouse the para residues were more important, which is in agreement with results from our docking analysis.

Furthermore, we tried to obtain a quantitative support to our indication. As a stating point a subset of aniline derivatives that comprise about 16% of all compounds in the model 2 training set was selected. Good correlations were found between the absolute value of the differences in carcinogenicity and the differences in the LBE values. This was a strong indication of relationship between CYP2E1 metabolism and the species differences in carcinogenicity for the selected chemicals. We also tried to quantitatively describe this process. Possible relationships between the LBE of the oxidation positions (Fig. 4) and carcinogenicity (i.e. not only for the differences in the carcinogenicity) were searched for. In the case of mouse LBE results a moderate correlation to carcinogenicity was found, which was significantly improved by exclusion of the *N*,*N*′-dimethylaniline as a strong outlier. There was no regression in the case of rat carcinogenicity. The reason can be the different enzyme residues, which are correlated to LBE values. For mouse CYP2E1 complexes the main contribution came from the heme (in particular the iron atom) and joined residues. For rat the chemicals were at larger distances from the heme. For most of the compounds an H-bound at the amino group change the lowest LBE values from para to ortho places. From this point of view the rat docking results provided a description of the process related but not directly linked to oxidation. There is a difficult transport to the heme and the rat docking results reflect this. Recently, similar results were obtained by docking technique for species-related differences in metabolism through CYP1A2 [60].

We studied the reason for the *N*,*N*′-dimethylaniline outlier (Sections 3.7 and 3.8.1) and found that the range of LBE values of methyl carbon atom binding to N atom differ to the range of LBE for C_{sp^2} when they are both randomly bound in various positions to the binding site. We notice that *N*,*N*′-dimethylaniline is atypical, compared to the other anilines studied in this set of compounds, because it is the only one with methyl groups linked to the nitrogen. This can explain the weak prediction of this chemical. Another influencing factor may come from the manner of LBE descriptor calculation is done. Indeed, the used parameterization in docking calculations may be not related to any binding processes, leading to "noise" in the results. The LBE values of the substituents are dependent from many computation factors (software score function, parameterization, etc.), but differences in LBE values for the same substituents are a relative quantity and relate more to the ligand-enzyme binding feature. Further studies should be done to check these factors. For instance, one could use residues (not individual atoms) LBE as a descriptor calculated by molecular mechanics or other techniques [61].

Furthermore, we tried to extend the significance of the metabolic process to most of benzene derivatives in our data set. We compared regions with significant regression levels on 3D-QSAR maps and LBE regression values toward carcinogenicity, at the same chemical positions for our subset of compounds. The results were less significant than in the case of LBE differences. A possible explanation can be related to the nature of the LBE descriptor. However, the most essential factor can be the alignment rules used for building of 3D-QSAR models. The molecules were aligned using the common phenyl ring as a template, based on well-known biophores, and the compounds' long chains were oriented mainly in one direction. The amino group has the same position in the aniline derivatives. Our docking results (Figs. 5–8) support this alignment: 3D-space position of phenyl ring in enzyme active sites is similar for each species and the long chains can be put only in one direction. However, we can see from Figs. 7 and 8 that the position of the amino group in 2,4-xylidine is the same as in aniline for mouse but differs in rat. Hence, according to our docking results we used wrong direction in the case of rat 2,4-xylidine alignment and changed the position of methyl and amino groups. We can expect a similar situation for some other small chemical residues in the used alignment. One of the popular approaches to solve this problem is structure-based 3D-QSAR using docking conformers for 3D-QSAR alignment [62]. In toxicology it is harder to apply this technique because the target receptors that mainly contribute to the variance of the data are often unknown. Moreover, for some of the chemicals other oxidation positions in CYP2E1 are likely, producing additional metabolites that are important for carcinogenicity differences too; in some cases, as shown in our docking results, there were two different metabolites produced, which have almost equal quantities, in agreement to the experimental data. However, as we demonstrated recently, when the aim is to compare species-related differences and identify the main ligand–receptor interaction, the use of docking conformers is not critical to obtain a sufficient match between 3D-QSAR, docking and LBE results [61]. Further help comes from 3D-QSAR and GRID maps comparison. As shown above, there was a noticeable similarity between carcinogenicity difference 3D-QSAR steric map and GRID CYP2E1 rat map. In all other maps only a slight relationship was found, similar to the carcinogenicity relationships with the oxidations positions LBE values and LBE-3D-QSAR comparison. However, all approaches independently show an influence of CYP2E1 enzyme metabolism not only to the differences in carcinogenicity, but also for mouse carcinogenicity. These results indicate that the weak correlations of LBE-3D-QSAR comparison and LBE for the oxidation positions probably come from the biological mechanism of action but not from the alignment approach.

The summarized results show that the CYP2E1 primary metabolism has an important role in species-related differences in carcinogenicity for a significant part of the benzene derivatives we studied. For some classes, like the aniline derivatives and other benzene derivatives, it is likely that CYP2E1 metabolism plays essential role in mouse carcinogenicity too. However, the post P450 transformation, DNA binding and many other processes are probably determinants for the carcinogenicity in many of the compounds. We believe that, to explain in detail the general carcinogenicity, many steps and combinations of approaches are required.

5. Conclusions

The present study generated high predictive 3D-QSAR models, which we used to predict carcinogenicity in mouse and rat, and their differences. 3D-QSAR maps enabled us to identify the chemical residues contributing to the species-related differences in carcinogenicity. Docking results for the oxidation mechanisms, supported by LBE values, provided a method for a quantitative description and prediction of metabolic processes and their relationship to carcinogenicity. We used this methodology to explain the species differences in carcinogenicity for a set of aniline derivatives. Furthermore, this approach could be helpful in development of new, more selective chemoprotective agents because the knowledge of the primary metabolic process of the carcinogenic chemicals gives a better idea on how to inhibit it. GRID method identified

the binding site features and itself proved helpful information. The results from 3D-QSAR and GRID maps comparison showed that this could be a helpful tool for a fast identification of the enzymes responsible for the differences in carcinogenicity and toxicity and together with the docking-LBE method helped to detail the species-related features. The combinations of all used methods can improve the knowledge of biochemical processes. Our study links 3D-QSAR, docking, LBE and GRID approaches. This enabled us to evaluate the contribution of CYP2E1 and describe the metabolic processes that can relate to differences in carcinogenicity.

Acknowledgements

We gratefully acknowledge support for this research from the IMAGETOX EC Project (HPRN-CT-1999-00015). Thanks due to Dr. Irini Doytchinova for Chem-X software and Elina Mihaylova for the helpful discussion.

Appendix A. Supplementary data

Supplementary data associated with this article can be found, in the online version, at doi:10.1016/j.jmgm.2008.04.004.

References

[1] G. Gini, M. Lorenzini, E. Benfenati, P. Grasso, M. Bruschi, Predictive carcinogenicity: a model for aromatic compounds, with nitrogen-containing substituents, based on molecular descriptors using an artificial neural network, J. Chem. Inf. Comp. Sci. 39 (1999) 1076–1080.
[2] K. Enslein, V.K. Gombar, B.W. Blake, Use of SAR in computer-assisted prediction of carcinogenicity and mutagenicity of chemicals by the TOPKAT program, Mutat. Res. 305 (1994) 47–61.
[3] R. Todeschini, P. Gramatica, R. Provenzani, E. Marengo, Weighted holistic invariant molecular descriptors. Part 2. Theory development and applications on modeling physicochemical properties of polyaromatic hydrocarbons, Chem. Intell. Lab. Syst. 27 (1995) 221–229.
[4] E. Benfenati, G. Gini, Computational predictive programs (expert systems) in toxicology, Toxicology 119 (1997) 213–225.
[5] G.P. Ford, J.D. Scribner, Prediction of nucleoside–carcinogen reactivity. Alkylation of adenine, cytosine, guanine, and thymine and their deoxynucleosides by alkanediazonium ions, Chem. Res. Toxicol. 3 (1990) 219–230.
[6] D.F. Lewis, C. Ioannides, D.V. Parke, A quantitative structure–activity relationship (QSAR) study of mutagenicity in several series of organic chemicals likely to be activated by cytochrome P450 enzymes, Teratogen. Carcin. Mut. 1 (2003) 187–193.
[7] W.E. Evans, M.V. Relling, Pharmacogenomics: translating functional genomics into rational therapeutics, Science 286 (1999) 487–491.
[8] D.F. Lewis, M. Dickins, Factors influencing rates and clearance in P450-mediated reactions: QSARs for substrates of the xenobiotic-metabolizing hepatic microsomal P450s, Toxicology 170 (2002) 45–53.
[9] R.J. Turesky, V. Parisod, T. Huynh-Ba, S. Langouët, F.P. Guengerich, Regioselective differences in *C*(8)- and *N*-oxidation of 2-amino-3,8-dimethylimidazo[4,5-*f*]quinoxaline by human and rat liver microsomes and cytochromes P450 1A2, Chem. Res. Toxicol. 14 (2001) 901–911.
[10] G. Sello, L. Sala, E. Benfenati, Predicting toxicity: a mechanism of action model of chemical mutagenicity, Mutat. Res. 479 (2001) 141–171.
[11] F.P. Guengerich, Common and uncommon cytochrome P450 reactions related to metabolism and chemical toxicity, Chem. Res. Toxicol. 14 (2001) 611–650.
[12] G.G. Gibson, P. Skett, Introduction to Drug Metabolism, Nelson Thornes Ltd., Cheltenham, 2001.
[13] M. Stiborová, E. Frei, M. Wiessler, H.H. Schmeiser, Human enzymes involved in the metabolic activation of carcinogenic aristolochic acids: evidence for reductive activation by cytochromes P450 1A1 and 1A2, Chem. Res. Toxicol. 14 (2001) 1128–1137.
[14] D.F. Lewis, M.G. Bird, D.V. Parke, Molecular modelling of CYP2E1 enzymes from rat, mouse and man: an explanation for species differences in butadiene metabolism and potential carcinogenicity, and rationalization of CYP2E substrate specificity, Toxicology 118 (1997) 93–113.
[15] T. Nakajima, R.S. Wang, E. Elovaara, S.S. Park, H.V. Gelboin, H. Vainio, Cytochrome P450-related differences between rat and mouse in the metabolism of benzene, toluene and trichloroethylene in liver microsomes, Biochem. Pharmacol. 45 (1993) 1079–1085.
[16] D.E. Hathway, Toxic action/toxicity, Biol. Rev. Camb. Philos. Soc. 75 (2000) 95–127.
[17] E.P. Gallagher, K.L. Kunze, P.L. Stapleton, D.L. Eaton, The kinetics of aflatoxin B1 oxidation by human cDNA-expressed and human liver microsomal cytochromes P450 1A2 and 3A4, Toxicol. Appl. Pharm. 141 (1996) 595–606.
[18] J.D. Kelly, D.L. Eaton, F.P. Guengerich, R.A. Coulombe, Aflatoxin B1 activation in human lung, Toxicol. Appl. Pharm. 144 (1997) 88–95.
[19] S. Langouët, B. Coles, F. Morel, L. Becquemont, P. Beaune, F.P. Guengerich, B. Ketterer, A. Guillouzo, Inhibition of CYP1A2 and CYP3A4 by oltipraz results in reduction of aflatoxin B1 metabolism in human hepatocytes in primary culture, Cancer Res. 55 (1995) 5574–5579.
[20] C. Cavin, C. Bezencon, G. Guignard, B. Schilter, Coffee diterpenes prevent benzo[*a*]pyrene genotoxicity in rat and human culture systems, Biochem. Biophys. Res. Commun. 306 (2003) 488–495.
[21] S. Bu, Y. Kim, S. Kim, M. Lee, Effects of enzyme inducers and inhibitor on the pharmacokinetics of intravenous 2-(allylthio) pyrazine, a new chemoprotective agent, in rats, Biopharm. Drug Dispos. 21 (2000) 157–164.
[22] L. Jin, T.A. Baillie, Metabolism of the chemoprotective agent diallyl sulfide to glutathione conjugates in rats, Chem. Res. Toxicol. 10 (1997) 318–327.
[23] K. Mahéo, F. Morel, S. Langouët, H. Kramer, E. Le Ferrec, B. Ketterer, A. Guillouzo, Inhibition of cytochromes P-450 and induction of glutathione *S*-transferases by sulforaphane in primary human and rat hepatocytes, Cancer Res. 57 (1997) 3649–3652.
[24] I. Gut, V. Nedelcheva, P. Soucek, P. Stopka, P. Vodicka, H.V. Gelboin, M. Ingelman-Sundberg, The role of CYP2E1 and 2B1 in metabolic activation of benzene derivatives, Arch. Toxicol. 71 (1996) 45–56.
[25] C.D. Klaassen, Casarett & Doull's Toxicology: The Basic Science of Poisons, McGraw-Hill, New York, 2001.
[26] D.J. McCarthy, W.R. Waud, R.F. Struck, D.L. Hill, Disposition and metabolism of aniline in Fischer 344 rats and C57BL/6 X C3H F1 mice, Cancer Res. 45 (1985) 174–180.
[27] E. Lo Piparo, F. Fratev, P. Mazzatorta, M. Smiesko, E. Benfenati, Toxicity in allelopathy: in silico approach, in: M.J. Reigosa, N. Pedrol, L. González (Eds.), Allelopathy: A Physiological Process with Ecological Implications, Springer, Berlin, 2006 , pp. 105–123 (Chapter 5).
[28] L.S. Gold, T.H. Slone, N.B. Manley, G.B. Garfinkel, E.S. Hudes, L. Rohrbach, B.N. Ames, The carcinogenic potency database: analyses of 4000 chronic animal cancer experiments published in the general literature and by the U.S. National Cancer Institute/National Toxicology Program, Environ. Health Perspect. 96 (1991) 11–15.
[29] M. Vracko, A study of structure–carcinogenicity relationship for 86 compounds from NTP database using topological indices as descriptors, SAR QSAR Environ. Res. 11 (2000) 103–115.
[30] Chem-X®, Chemical Design Ltd., Roundway House, Cromwell Parek, Chipping Norton, Oxfordskire OX 75 SR, UK, July 1999.
[31] HyperChem®, Hypercube Inc., 1115 NW 4th Street, Gainesville, FL 32601, USA.
[32] J.P. Stewart, Optimization of parameters for semiempirical methods. I. Method, J. Comput. Chem. 10 (1989) 209–220.
[33] X. Chen, A. Christopher, J. Jones, Q. Guo, F. Xu, R. Cao, L.-L. Wong, Z. Rao, Crystal structure of the F87W/Y96F/V247L mutant of cytochrome P-450cam with 1,3,5-trichlorobenzene bound and further protein engineering for the oxidation of pentachlorobenzene and hexachlorobenzene, J. Biol. Chem. 277 (2002) 37519–37526.
[34] R. Raag, B.A. Swanson, T.L. Poulos, P.R. Ortiz de Montellano, Formation, crystal structure, and rearrangement of a cytochrome P-450cam iron-phenyl complex, Biochemistry 29 (1990) 8119–8126.
[35] D.F. Lewis, B.G. Lake, M. Dickins, Y.F. Ueng, P.S. Goldfarb, Homology modelling of human CYP1A2 based on the CYP2C5 crystallographic template structure, Xenobiotica 33 (2003) 239–254.
[36] M.J. Don, D.F. Lewis, S.Y. Wang, M.W. Tsai, Y.F. Ueng, Effect of structural modification on the inhibitory selectivity of rutaecarpine derivatives on human CYP1A1, CYP1A2, and CYP1B1, Bioorg. Med. Chem. Lett. 13 (2003) 2535–2538.
[37] D.F. Lewis, M.G. Bird, M. Dickins, B.G. Lake, P.J. Eddershaw, M.H. Tarbit, P.S. Goldfarb, Molecular modelling of human CYP2E1 by homology with the CYP102 haemoprotein domain: investigation of the interactions of substrates and inhibitors within the putative active site of the human CYP2E1 isoform, Xenobiotica 30 (2000) 1–25.
[38] D.F. Lewis, B.G. Lake, M.G. Bird, G.D. Loizou, M. Dickins, P.S. Goldfarb, Homology modelling of human CYP2E1 based on the CYP2C5 crystal structure: investigation of enzyme–substrate and enzyme–inhibitor interactions, Toxicol. In Vitro 17 (2003) 93–105.
[39] D.F. Lewis, Homology modelling of human CYP2 family enzymes based on the CYP2C5 crystal structure, Xenobiotica 32 (2002) 305–323.
[40] D.F. Lewis, B.G. Lake, Species differences in coumarin metabolism: a molecular modelling evaluation of CYP2A interactions, Xenobiotica 32 (2002) 547–561.
[41] D.R. Ferro, J. Hermans, A different best rigid-body molecular fit routine, Acta Crystallogr. A 33 (1977) 345–347.
[42] K.H. Kim, 3D QSAR in Drug Design Recent Advances, Kluwer/E SCOM, London, 1998.
[43] A. Cavalli, G. Greco, E. Novelliono, M. Recanatini, Linking CoMFA and protein homology models of enzyme–inhibitor interactions: an application to non-steroidal aromatase inhibitors, Bioorg. Med. Chem. 8 (2000) 2771–2780.
[44] B. Boeckmann, A. Bairoch, R. Apweiler, M.-C. Blatter, A. Estreicher, E. Gasteiger, M.J. Martin, K. Michoud, C. O'Donovan, I. Phan, S. Pilbout, M. Schneider, The SWISS-PROT protein knowledge base and its supplement TrEMBL in 2003, Nucl. Acids Res. 31 (2003) 365–370.

[45] H.M. Berman, J. Westbrook, Z. Feng, G. Gilliland, T.N. Bhat, H. Weissig, I.N. Shindyalov, P.E. Bourne, The protein data bank, Nucl. Acids Res. 28 (2000) 235–242.
[46] K. Ginalski, A. Elofsson, D. Fischer, L. Rychlewski, 3D-Jury: a simple approach to improve protein structure predictions, Bioinformatics 22 (2003) 1015–1018.
[47] K. Ginalski, J. Pas, S.L. Wyrwicz, M. Grotthuss, J.M. Bujnicki, L. Rychlewski, ORFeus: detection of distant homology using sequence profiles and predicted secondary structure, Nucl. Acids Res. 31 (2003) 3804–3807.
[48] M.A. Marti-Renom, A. Stuart, A. Fiser, R. Sánchez, F. Melo, A. Sali, Comparative protein structure modeling of genes and genomes, Annu. Rev. Biophys. Biomol. Struct. 29 (2000) 291–325.
[49] W.D. Cornell, P. Cieplak, C.I. Bayey, I. Gould, T.K.M. Merz, D.M. Ferguson, D. Spellmeyr, T. Fox, J.W. Caldmell, P.A. Kollman, Second generation force field for the simulation of proteins, nucleic acids, and organic molecules, J. Am. Chem. Soc. 117 (1995) 5179–5197.
[50] G.M. Morris, D.S. Goodsell, R.S. Halliday, R. Huey, W.E. Hart, R.K. Belew, A.J. Olson, Automated docking using a Lamarckian genetic algorithm and empirical binding free energy function, J. Comput. Chem. 19 (1998) 1639–1662.
[51] P.J. Goodford, GRID 21, Molecular Discovery Ltd., University of Oxford, England, SGI.
[52] SIMCA, Umetrics AB, Box 7960, S-90719 Umea, Schweden.
[53] G.-D. Xuan, Z.-Q. Liu, Cytochrome P450 metabolic intermediate formation from *p*-chloro-*o*-toluidine as a possible new probe to characterize cytochrome P450 IIB, Chin. J. Pharmacol. Toxicol. 9 (1995) 3–7.
[54] C. Leslie, G.F. Reidy, M. Murray, N.H. Stacey, Induction of xenobiotic biotransformation by the insecticide chlordimeform, a metabolite 4-chloro-*o*-toluidine and a structurally related chemical *o*-toluidine, Biochem. Pharmacol. 37 (1988) 2529–2535.
[55] R.N. Pandey, A.P. Armstrong, P.F. Hollenberg, Oxidative *N*-demethylation of *N*,*N*-dimethylaniline by purified isozymes of cytochrome P-450, Biochem. Pharmacol. 38 (1989) 2181–2185.
[56] K.L. Cheever, D.E. Richards, H.B. Plotnick, Metabolism of *ortho*-, *meta*-, and *para*-toluidine in the adult male rat, Toxicol. Appl. Pharm. 56 (1980) 361–369.
[57] J. Gan, P.L. Skipper, S.R. Tannenbaum, Oxidation of 2,6-dimethylaniline by recombinant human cytochrome P450s and human liver microsomes, Chem. Res. Toxicol. 14 (2001) 672–677.
[58] B. Przybojewska, Assessment of aniline derivatives-induced DNA damage in the liver cells of B6C3F1 mice using the alkaline single cell gel electrophoresis ('comet') assay, Cancer Lett. 147 (1999) 1–4.
[59] P.A. Williams, J. Cosme, A. Ward, H.C. Angove, D. Matak Vinkovic, H. Jhoti, Crystal structure of human cytochrome P450 2C9 with bound warfarin, Nature 424 (2003) 464.
[60] J.C. Prasad, Docking to large ensembles of homology models reliably explains the substrate binding differences in cytochrome P450 1As of human and fish species, in: The 229th ACS National Meeting, Poster 173, San Diego, CA, 13-17 March, 2005.
[61] F. Fratev, E. Benfenati, 3D-QSAR and molecular mechanics study for the differences in the azole activity against yeast like and filamentous fungi and their relation to P450DM inhibition. 1. 3-Substituted-4(3*H*)-quinazolinones, J. Chem. Inf. Model. 45 (2005) 634–644.
[62] W. Sippl, Development of biologically active compounds by combining 3D QSAR and structure-based design methods, J. Comput. Aided Mol. Des. 16 (2002) 825–830.